Hindawi
International Journal of Aerospace Engineering
Volume 2023, Article ID 5934333, 14 pages
https://doi.org/10.1155/2023/5934333

Research Article

High Cycle Fatigue Life Prediction of Single-Crystal Specimen Based on TCD Method and Crystal Plasticity Theory

Yunwu Wu,[1] Yixiong Liu,[1,2] Wei Wang,[1] Ying Li,[1] and Rui Geng[1]

[1]*AECC Shenyang Engine Research Institute, Shenyang 110015, China*
[2]*Northwestern Polytechnical University, Xi'an, 710072, China*

Correspondence should be addressed to Yixiong Liu; yixiong.liu5021@gmail.com

Received 2 September 2022; Revised 1 January 2023; Accepted 5 January 2023; Published 19 January 2023

Academic Editor: Antonio Concilio

This paper performs a comprehensive investigation on the high cycle fatigue (HCF) life prediction of turbine blade with film cooling holes. The modified theory of critical distance (MTCD) method is proposed to estimate the fatigue life of the specimen considering the notch sensitivity coefficient and multiaxial stress effect. Then, two types of specimens were designed with regard to the single-hole and multihole conditions. Afterwards, the dangerous path and fatigue life of the two specimens were achieved implementing the MTCD method. Then, the experiments and failure analysis were carried out. The results show that the stress concentration and multiaxial stress resulting from the film cooling holes are the primary reasons that the cracks originated. Meanwhile, the dangerous path of the single-hole specimen is quite different from the multihole specimen due to the interhole interference. Finally, most of the calculated fatigue life is within the twice error band of the tested life.

1. Introduction

Nowadays, the increasing thrust demand has called for high turbine entry temperature (TET) and wide-range rotational speed of modern turbofan engine [1]. Consequently, the turbine blade works in a harsh environment and might experience fatigue failure. To be specific, the high temperature and high speed would generate very high stress concentration at the film cooling holes and some sharp edges, especially for the hollow blade. Besides, the notch effect cannot be ignored when the turbine blade employs many holes and fins. It would not only aggravate the stress concentration but also generate multiaxial stress [2] due to the existence of the holes. Meanwhile, the implementation of single-crystal materials on turbine blade also contributes to the failures since the crystal defects are inevitable [3]. Many studies show that the turbine blades are vulnerable to high cycle fatigue (HCF) failures [4–7]. Therefore, the prediction of fatigue life of turbine blade is crucial to guarantee a safety operation.

The theory of critical distance (TCD) method was first proposed by Neuber [8] and Peterson [9] and developed by Susmel and Taylor [10] and Taylor [11]. It provides a deep insight into the estimation of fatigue limit and evaluates the fatigue damage using the linear elastic stress field in the crack initiation region. By introducing the characteristic distance related to material properties and loading conditions [11], the notch sensitivity of the specimen is linked to local damage. It should be pointed out that the TCD method is applicable in both monotonous load and periodic load [12]. Furthermore, the point method (PM) and line method (LM) are most widely accepted whereas the area method (AM) and volume method (VM) are seldom used due to the complexity. It was reported by Taylor and Wang [13] that PM demonstrated the highest accuracy in predicting various forms of notched specimens. In recent years, it is often combined with the improved Wöhler curve method [14] to tackle the fretting fatigue issues [15–19]. Based on the multiaxial fatigue criterion and PM, Ronchei et al. [20] introduced the critical plane to evaluate the metal component life under fretting load. Another application of TCD method is the residual compressive stress assessment using the LM. It has been verified in high residual stress gradient cases [21, 22].

The TCD method is commonly accepted and implemented in the field of notch fatigue analysis. Susmel [23] reviewed the utilization of TCD method in the fatigue field and extended

the usage of TCD method to torsional fatigue of notched specimens [24]. Besides, the accuracy of TCD theory in HCF mechanical model was investigated [25]. Liao et al. [26] summarized 8 life assessment procedures and verified the optimal one with experiments. Then, a systematical review was made focusing on the notch fatigue concerning the stress gradient effect [27]. Afterwards, the TCD method was compared with highly stressed volume (HSV) and weakest link theory (WLT) with regard to GH4169 specimen fatigue life prediction [28]. Jadallah et al. [29] made an improvement in the traditional TCD method and verified it by HCF tests. Different notch stress concentration factors were experimented with the adopted microstructure length of the material as a parameter combined with the gradient elasticity theory. Chen [30] implemented the LM to estimate the notch fatigue limit from both energy condition and crack propagation condition perspectives. Razavi et al. [31] investigated the fatigue lifetime of 3D-printed titanium alloy Ti6Al4V while the specimen and the notch were kept as the manufacturing condition.

One of the tough tasks remaining to be solved is to precisely predict the elastic-plastic stress and strain field resulting from the anisotropy of single-crystal alloy [32, 33]. Continuous studies on the constitutive of single-crystal alloy are still carried out around the world. Typically, it can be divided into phenomenological model and crystal slip model. The former is represented by Hill and Hill and Rice [34, 35] and mainly starts from the modified cubic symmetric anisotropy constitutive model. This model is based on macroscopic stress and strain and cannot reflect the true deformation of materials. Therefore, it is difficult to establish an accurate description of the crystal anisotropy and orientation sensitivity. The crystal plasticity theory based on the slip system was first developed by Taylor [36, 37]. This model reveals the relationship between shear stress and strain rate of slip system with time, which can better track the change of plastic anisotropy.

In this paper, a design process is proposed to achieve the turbine blade fatigue life with film cooling holes. The modified TCD is derived considering the notch sensitivity coefficient and multiaxial stress effect. Then, two types of specimens are designed with different holes. The fatigue life of the specimen is predicted with the proposed TCD method and the dangerous path is obtained. Afterwards, the experiment is carried out to verify the calculation results.

2. Methodology

2.1. Design Framework. In this scenario, the main purpose is to develop a modified TCD method to precisely predict the HCF life of the concerned component with film cooling holes. A systematic design framework is proposed to better demonstrate the work, as depicted in Figure 1. The first step is to introduce the film cooling hole notch parameter and multiaxial stress parameter to improve the accuracy of conventional TCD method. The impacts of film cooling holes and hole number are adopted in the component life prediction. Afterwards, the simulating specimen is designed to simulate the turbine blade with file cooling holes. It should be noted that both the single-hole and multihole specimens are considered for a fair comparison. The dangerous path is predicted according to the combination of finite element analysis and the modified TCD approach. It would provide a good opportunity to observe the stress concentration of the film cooling holes. Meanwhile, the dangerous path is estimated from the test and failure analysis results. The comparisons of the simulation and test would verify the accuracy and reliability of the proposed method. Finally, the predicted life is achieved and compared with the tested life, whereas the error band is obtained which would also validate the proposed method.

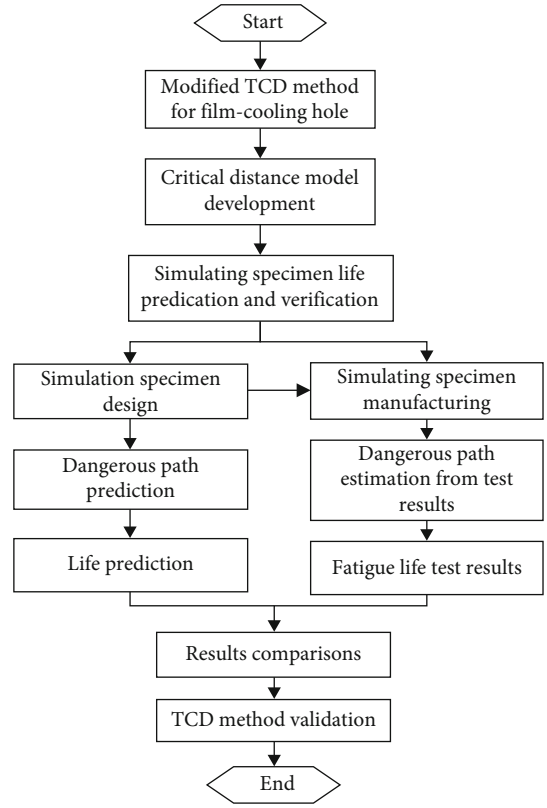

Figure 1: Design framework.

2.2. Modified TCD Method

2.2.1. Conventional TCD Method. Convectional TCD method is mainly used to calculate the fatigue life under multiaxial stress. The fundamental principle of fracture mechanism is that the fatigue crack originates from the maximum stress concentration location (MSCL) and propagates along the dangerous path until it ruptures. To be specific, when the stress decreases to a certain value along a dangerous path, the structure encounters failure. The determinant stress is defined as the equivalent stress σ_{eff} that equals the fatigue limit of the material. It decides the distribution of maximum principal stress in the stress concentration area.

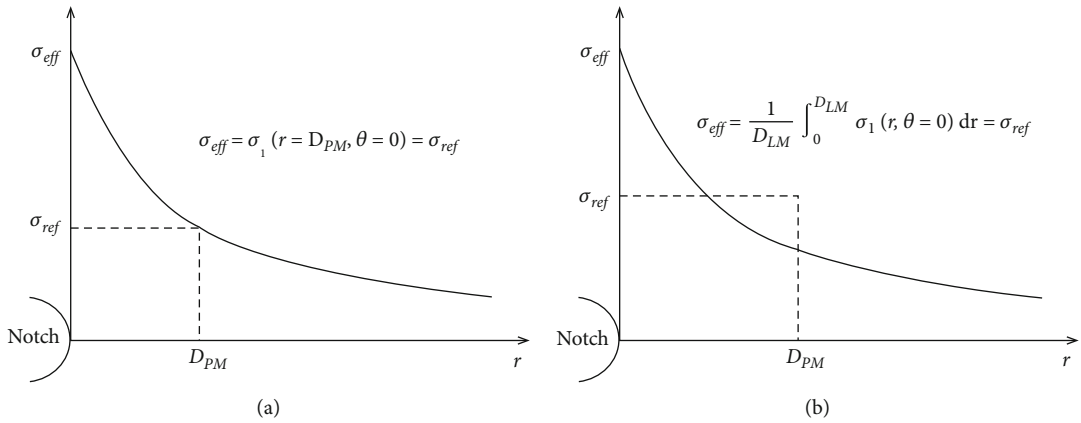

Figure 2: Schematic diagram of PM (a) and LM (b).

Tanaka and Taylor pointed out that the equations of PM and LM could be arranged as follows:

$$\begin{aligned} \sigma_{\text{eff}} &= \sigma_1 (r = D_{\text{PM}}, \theta = 0) = \sigma_{\text{ref}}, \\ \sigma_{\text{eff}} &= \frac{1}{D_{\text{LM}}} \int_0^{D_{\text{LM}}} \sigma_1 (r, \theta = 0) dr = \sigma_{\text{ref}}, \end{aligned} \tag{1}$$

where σ_1 is the maximum principal stress, σ_{ref} is the reference equivalent stress, σ_{eff} is the equivalent stress, D_{LM} is the critical distance of line method, and D_{PM} is the critical distance of point method.

Regarding the HCF issues, the parameters in the above equations can be defined by fatigue stress amplitude and gradient. Figure 2 depicts the schematic diagram of PM and LM under elastic stress distribution. It indicates that the specimen would reach the fatigue limit when the distance away from the MSCL approaches the D_{PM} or D_{LM} at the dangerous path. For the conventional TCD method, the determination of critical distance D_{PM} and D_{LM} is highly dependent on the material properties and stress ratio.

In order to calculate the critical distance in a more convenient way, Susmel and Taylor [38] came up with the characteristic distance L dependent on the critical stress intensity gradient ΔK_{th} and material fatigue limit σ_0, as shown in

$$L = \frac{1}{\pi} \left(\frac{\Delta K_{th}}{\sigma_0} \right)^2. \tag{2}$$

For PM and LM, the relationship between characteristic distance and critical distance is described as follows:

$$\begin{aligned} D_{PM} &= \frac{L_0}{2}, \\ D_{LM} &= 2L_0. \end{aligned} \tag{3}$$

Then, the fatigue life prediction model of the component is derived, as depicted in (4). It could be seen that the fatigue life is only related to L, A, and b, where A and b are decided by the material property and stress ratio.

$$L_{N_f} = A_{N_f}{}^b. \tag{4}$$

For the failure under static loading, the critical distance is defined in (5). The main difference between (2) and (5) is that the ΔK_{th} and σ_0 are substituted with K_{IC} and σ_{ref}, where K_{IC} represents the plane fracture toughness of the material.

$$L_S = \frac{1}{\pi} \left(\frac{K_{\text{IC}}}{\sigma_{\text{ref}}} \right)^2. \tag{5}$$

2.2.2. Modified TCD Method. According to the smooth specimen curve, when the material is in the initial stage of the fatigue cycle, N_f equals N_S. Equation (5) could be rewritten as

$$L(N_S) = L_S = \frac{1}{\pi} \left(\frac{K_{\text{IC}}}{\sigma_{\text{UTS}}} \right)^2. \tag{6}$$

However, when the material reaches the fatigue limit, that is, $N_f = N_0$ and substitute it into (5), then Equation (7) is obtained.

$$L(N_0) = \frac{1}{\pi} \left(\frac{K_{\text{IC}}}{\sigma_0} \right)^2. \tag{7}$$

According to (6) and (7), the values of parameters A and b are obtained as follows:

$$\begin{aligned} b &= \frac{\log (L_0/L_S)}{\log (N_0/N_S)}, \\ A &= \text{LN}_0{}^{-b}. \end{aligned} \tag{8}$$

It can be seen from (8) that A and b can be obtained once the N_0 and N_S are determined. Afterwards, the relationship

Table 1: Notch sensitivity coefficient under different conditions.

T (°C)	900 (single hole)	980 (single hole)	980 (multi hole)	1050 (single hole)
q_f	0.012	0.085	0.182	0.227

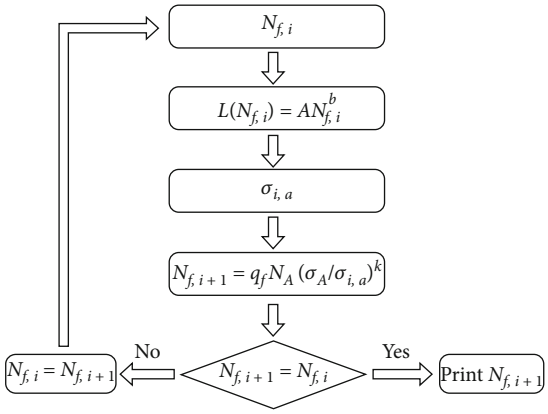

Figure 3: Flow chart of HCF life prediction by MTCD method.

between critical distance and fatigue life is established. It could be implemented to predict the HCF life of the component.

Nevertheless, it is not accurate to predict the fatigue life of the notch specimen using the largest stress gradient or the hot point [24]. In this scenario, the notch sensitivity coefficient q_f is adopted to include the effects of notches on the fatigue life. As presented in (9), notch factor q_f is determined by the theoretical stress concentration factor K_t and the fatigue strength ratio of smooth to notched specimens K_f. Also, the multiaxial stress effect is also taken into consideration by introducing the factor λ, acting as the exponent. It should be noted that λ used to be setting as 1.

The variance of q_f with temperature of the single-hole specimen is achieved and listed in Table 1. Meanwhile, the q_f of the multihole case is listed at temperature 980°C.

$$q_f = \left(\frac{K_f - 1}{K_t - 1}\right)^{\lambda}. \tag{9}$$

Figure 3 presents the work flow chart of calculating the HCF life implementing the modified theory of critical distance (MTCD) method. The first step is to assume an estimated fatigue life $N_{f,i}$, which needs to be as close as to the real life in order to reduce the iterations. It could be assumed according to the life of similar structure with equivalent stress level. After that, the maximum principal stress distribution along the dangerous path near the notch would be obtained using the PM approach. Consequently, the maximum principal stress at the location $L(N_{f,i})/2$ away from the notch tip would be achieved and denoted as $\sigma_{i,a}$, which is considered as the equivalent stress. Then, the q_f is introduced into the iteration $N_{f,i+1} = q_f \times N_A(\sigma_A/\sigma_{i,a})^k$, and the loop continues until $N_{f,i+1}$ equals N_f. This ensures that the

Table 2: Model parameters.

Parameters	Symbols	900°C	980°C	1050°C
Yield stress (MPa)	σ_y	895.4	680.0	493.3
Reference shear stress (MPa)	$g_{\alpha 0}$	365.5	277.6	201.4
Elastic modulus (MPa)	E	91830	80530	69300
Shear modulus (MPa)	G	97200	85600	90000
Poisson ratio	μ	0.386	0.390	0.399
Reference shear strain rate (s_{-1})	$\dot{r}_0^{(a)}$	0.003	0.003	0.003
Strain rate sensitivity	m	0.02	0.02	0.02
Hardening modulus (MPa)	h_0	434.5	312.0	204.8
Correction stress (MPa)	τ_s	300.0	296.4	293.3
Correction parameter	β	1.3	1.3	1.3

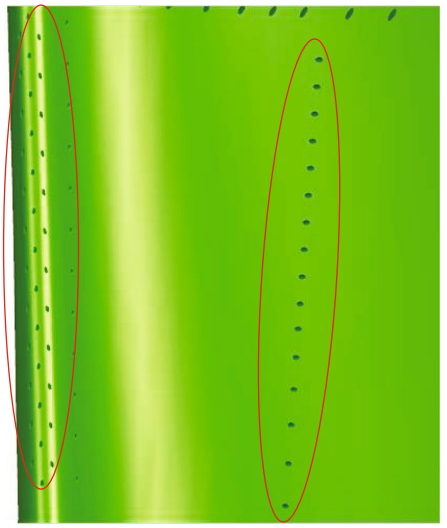

Figure 4: Demonstration of the turbine blade film cooling holes.

impacts of film cooling hole and multiaxial stress are considered in the turbine blade life prediction.

2.2.3. Elastic-Plastic Model Based on Crystal Plasticity Theory. In this scenario, the elastic-plastic constitutive model based on crystal plasticity theory is utilized to calculate the dangerous path in finite element analysis. The constitutive model of crystal plastic model was developed by Taylor. The total deformation gradient F is divided into two parts: elastic and plastic, as described in

$$F = F^e F^p. \tag{10}$$

When the crystal is deformed and twisted, the lattice vector changes and the slip direction $m^{(\alpha)}$ can be defined as

$$m^{*(\alpha)} = F^e m^{(\alpha)}. \tag{11}$$

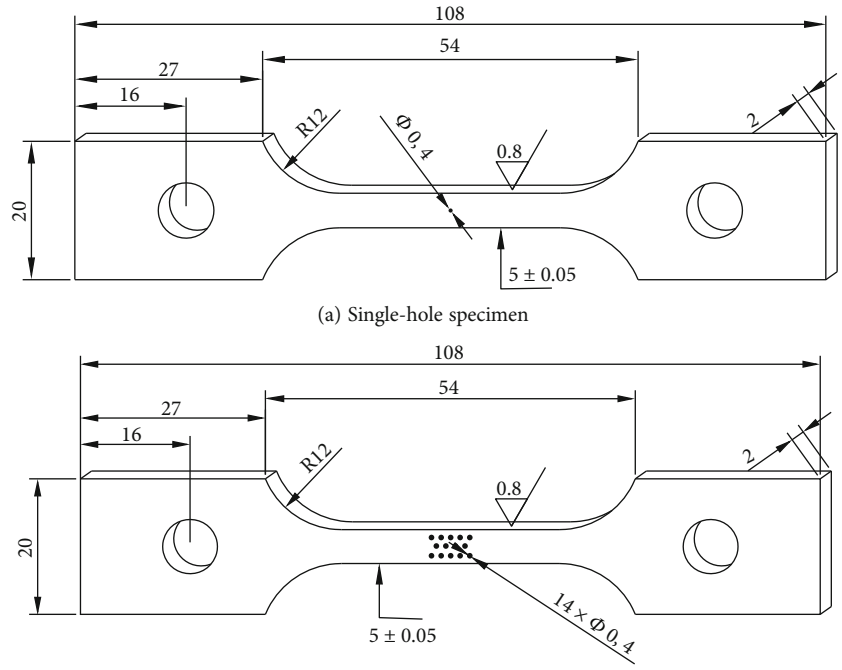

(a) Single-hole specimen

(b) Multihole specimen

Figure 5: The designed specimens for the experiment.

The normal vector $n^{*(\alpha)}$ of the slip face is listed as follows:

$$n^{*(\alpha)} = \left(\left(F^e\right)^{-1}\right)^T n^{(\alpha)}. \tag{12}$$

The velocity gradient is given by the standard equation:

$$L = \dot{F}F^{-1} = \dot{F}^*\left(F^*\right)^{-1} + F^*\dot{F}^p\left(F^p\right)^{-1}\left(F^*\right)^{-1}. \tag{13}$$

L can also be expressed as

$$L = D + W, \tag{14}$$

where D is the deformation rate tensor and W is the rotation tensor.

The plastic deformation consists of dislocations and slips:

$$L^p = \sum_{\alpha=1}^{N} P^{(\alpha)}\dot{\gamma}^{(\alpha)}, \tag{15}$$

where $\dot{\gamma}^{(\alpha)}$ is the slip rate of slip system α and $P^{(\alpha)}$ is the Schmidt factor of slip system α, which can be defined as

$$P^{(\alpha)} = \frac{1}{2}\left(m^{*(\alpha)} \otimes n^{*(\alpha)} + n^{*(\alpha)} \otimes m^{*(\alpha)}\right). \tag{16}$$

Furthermore, the Cauchy stress tensor is represented by σ, and the weighed Cauchy stress tensor is expressed by τ. The relationship between the two factors is listed as follows:

$$\begin{aligned} \tau &= (\det F)\sigma, \\ T &= F^e\tau F^{e-1}. \end{aligned} \tag{17}$$

The shearing stress is a component of the traction force along the slip direction, and it is related to the Cauchy stress through the Schmidt tensor.

$$\tau^{(\alpha)} = P^{(\alpha)} : T. \tag{18}$$

The strain rate is expressed by a power function equation:

$$\dot{\gamma}^{(\alpha)} = \dot{\gamma}_0^{(\alpha)}\left[\frac{\tau^{(\alpha)}}{g^{(\alpha)}}\right]\left[\left|\frac{\tau^{(\alpha)}}{g^{(\alpha)}}\right|\right]^{(1/m)-1}, \tag{19}$$

where $\dot{\gamma}_0^{(\alpha)}$ is the reference shear strain rate, m is the strain rate sensitivity index, and $g^{(\alpha)}$ is the reference shear stress which characterizes the current strain hardening state of the crystal and depends on the sum of the slip shear rate γ:

$$g^{(\alpha)} = g^{(\alpha)}(\gamma), \tag{20}$$

where γ is cumulative slip strain:

$$\gamma = \sum_{\alpha}\left|\gamma^{(\alpha)}\right|. \tag{21}$$

In order to simplify the calculation, the strain hardening of the materials can be replaced by the evolution equation of $g^{(\alpha)}$:

$$\dot{g}^{(\alpha)} = \sum_{\beta} h_{\alpha\beta}\left|\dot{\gamma}^{(\beta)}\right|. \tag{22}$$

In the equation, $h_{\alpha\beta}$ is a function of γ, which determines the hardening of slip system α caused by the amount of slip

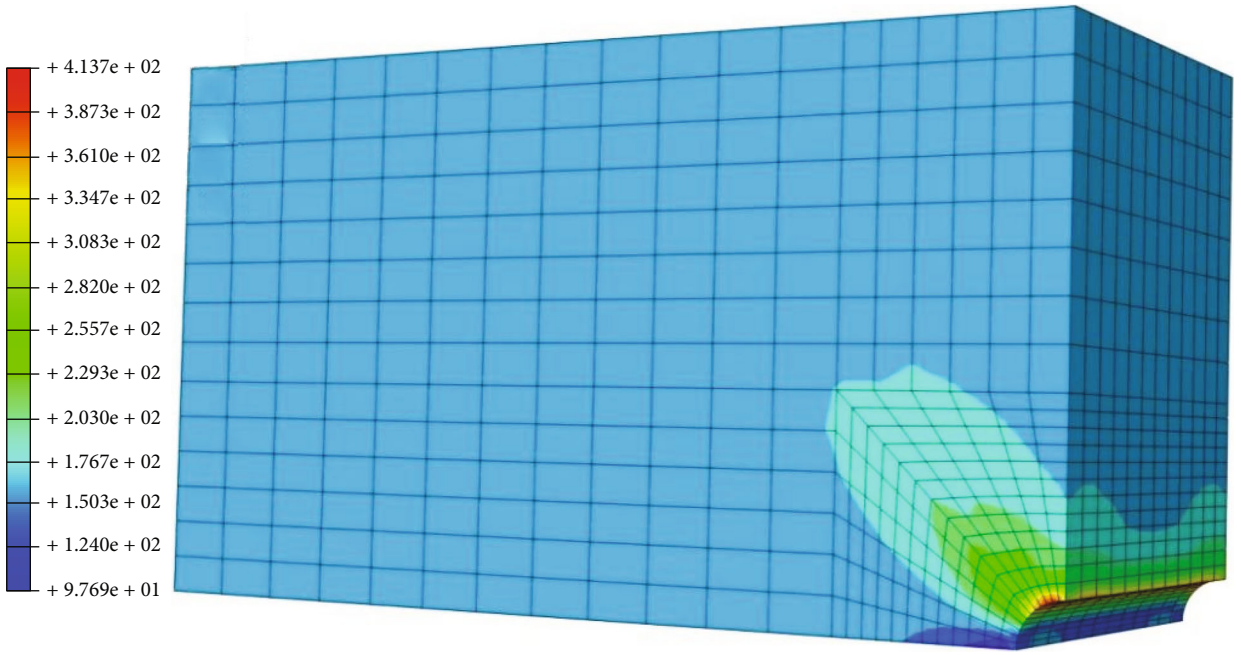

Figure 6: Maximum principal shear stress distribution of single-hole specimen (unit: MPa).

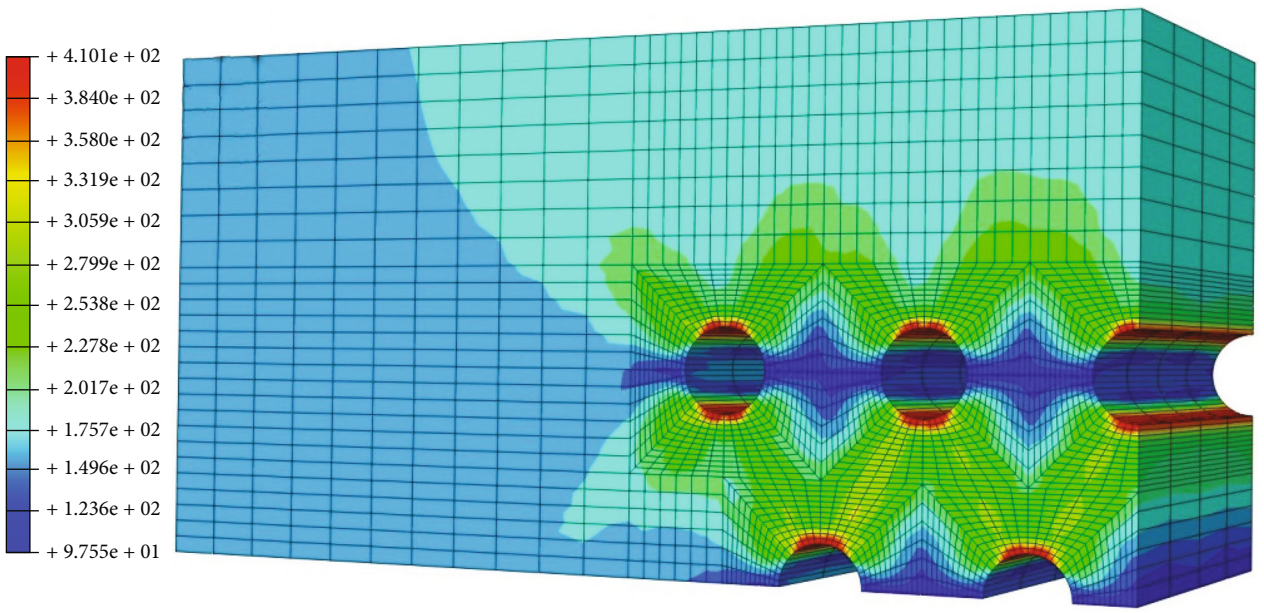

Figure 7: Maximum principal shear stress distribution multihole specimen (unit: MPa).

shear in slip system β, which can be obtained by the following formula:

$$h_{\alpha\beta} = q_{\alpha\beta} h_{\beta}, \tag{23}$$

where $q_{\alpha\beta}$ is the hardening coefficient and h_{β} is the hardening rate:

$$h_{\beta} = h_0 \left(1 - \frac{g_{\alpha}}{\tau_s}\right)^{\beta}, \tag{24}$$

where h_0 is the hardening modulus and τ_S and β are the model parameters.

In this scenario, the tensile tests were carried out to obtain the model parameters of (24) [39, 40]. The parameters are listed in Table 2. Meanwhile, the data is transported to ABAQUS as user-defined subroutine.

3. Simulating Specimen Life Prediction

3.1. Simulating Specimen Design. As presented in Figure 4, the film cooling holes are employed to cool the turbine

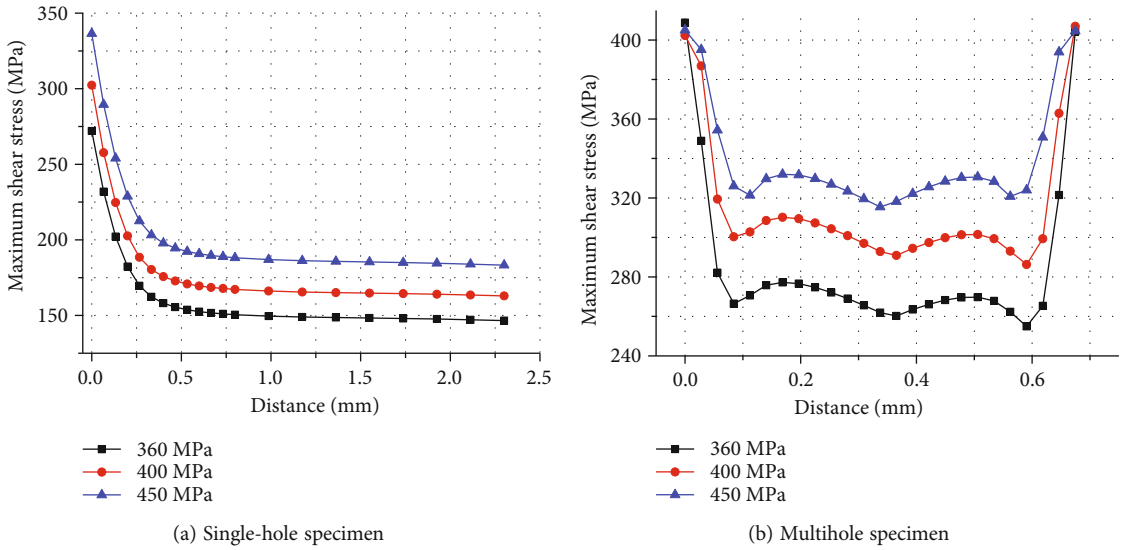

(a) Single-hole specimen (b) Multihole specimen

Figure 8: Maximum shear stress along the dangerous path.

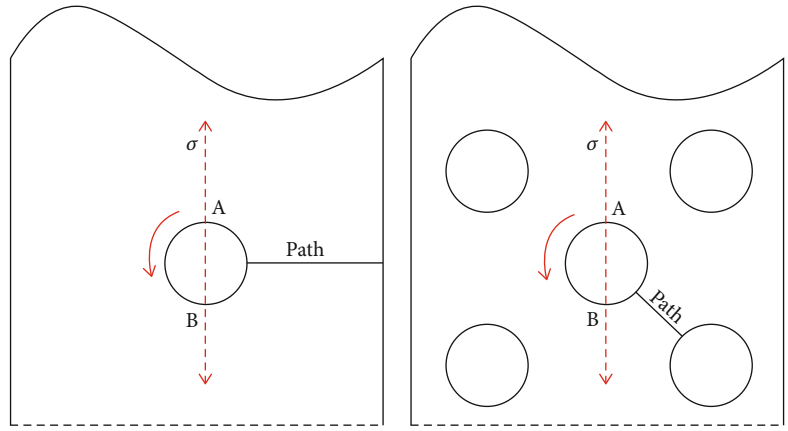

(a) Single-hole specimen (b) Multihole specimen

Figure 9: Dangerous path of the simulation results.

blade. Typically, there exists a high stress concentration at the film cooling holes area, which might pose HCF failure risk. In order to verify the proposed method, two types of specimens with film cooling holes are designed to simulate the turbine blade. The details of the specimen are presented in Figure 5. It can be seen clearly that the diameters of specimen with single hole and multihole are 0.4 mm, maintaining the same as the turbine blade film cooling holes. Meanwhile, two through-holes are observed at each specimen for the tensile cyclic loading. The thickness of the specimen is 2 mm while the radius of the transition area is 12 mm. It should be noted that the material remains nickel-based single-crystal superalloy DD6. To be specific, the tensile axis direction is [001] orientation while the thickness direction (the axial direction of the hole) is [010] orientation, and the width direction is [100] orientation. Besides, the orientation angle deviation is less than ±5°.

Table 3: Parameters of critical distance equation.

T (°C)	900 (single hole)	980 (single hole)	980 (multi hole)	1050 (single hole)
A	24.28	10.58	1.47	3.39
b	-0.054	-0.077	-0.118	-0.123

3.2. Dangerous Path Prediction. Finite element analysis is performed to calculate the dangerous path using the model parameters generated in Table 2. Considering the temperature of the turbine blade film cooling hole reaches about 980°C, the data implemented in the analysis also chooses the 980°C model parameters. The maximum shear stress distribution of the single-hole and multihole specimens is depicted in Figures 6 and 7. An obvious observation is that the maximum shear stress of the single-hole specimen lies

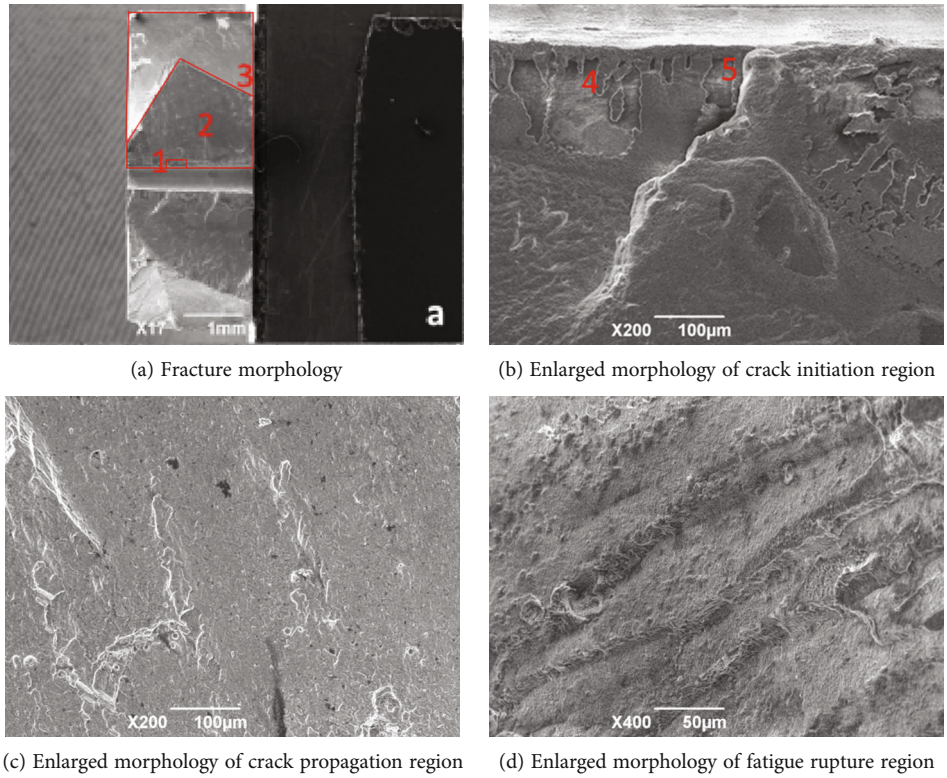

(a) Fracture morphology (b) Enlarged morphology of crack initiation region

(c) Enlarged morphology of crack propagation region (d) Enlarged morphology of fatigue rupture region

Figure 10: Fracture morphology of single-hole specimen.

at the middle region of the single hole whereas the maximum stress occurs near the hole edges.

Figure 8 depicts the maximum shear stress along the dangerous path. The crack would originate from the maximum stress and propagate along the dangerous path. For the single-hole specimen, the maximum shear stress decreased rapidly along the dangerous path from 0 to 0.5 mm. Then, it demonstrates a stable trend until 2.3 mm. Nevertheless, for the multihole specimen, the maximum principal stress first increases and peaks at 0.35 mm. Afterwards, it goes up to the maximum stress value at the hole edge and presents a saddle-like shape curve. Figure 9 presents the calculated dangerous path of both the single-hole specimen and multihole specimens. The main difference is that the dangerous path of the single-hole specimen is normal to the tensile stress whereas it is the connecting line of the center hole and side hole.

3.3. Life Prediction. According to the maximum principal stress distribution and the calculated dangerous path, the MTCD method is utilized to predict the HCF life of the specimen. The parameters of critical distance under temperatures are obtained and listed in Table 3.

Equations (25)–(28) present the relationship between life cycles and notch factor and critical distance of the single-hole and multihole specimens. It should be noted that when TCD method is implemented to predict the fatigue life, the two parameters A and b in the equation are determined by the material properties and the stress ratio of HCF experiments. Considering that the hole drill process has little impact on the macroscopic tensile properties of the specimens, it is not included in the developed model and the HCF life prediction.

$$\text{Single hole/900°C}: L(N_f) = 24.28 q_f(N_f)^{-0.054}, \quad (25)$$

$$\text{Single hole/980°C}: L(N_f) = 10.58 q_f(N_f)^{-0.077}, \quad (26)$$

$$\text{Single hole/1050°C}: L(N_f) = 3.39 q_f(N_f)^{-0.123}, \quad (27)$$

$$\text{Multihole/980°C}: L(N_f) = 1.47 q_f(N_f)^{-0.118}. \quad (28)$$

4. Experiment Verification

4.1. Failure Analysis. In this scenario, the fatigue test is carried out of the single-hole and multihole specimens under tensile stress loading. By implementing the stress-controlled loading mode, the axial tension-tension HCF experiments with a stress ratio of 0.1 are undertaken. The cyclic loading frequency is within 80-90 Hz. The specimens with single-film cooling holes are tested at 900°C, 980°C, and 1050°C whereas the cases with multi-film cooling holes are tested at 980°C.

The morphology of the single-hole fracture is depicted in Figure 10. The crack initiation region 1, propagation region 2, and final rupture region 3 are clearly observed in Figure 10(a). Meanwhile, two distinct areas with different colors are identified due to the oxidation effects. As expected, the crack initiation and propagation regions

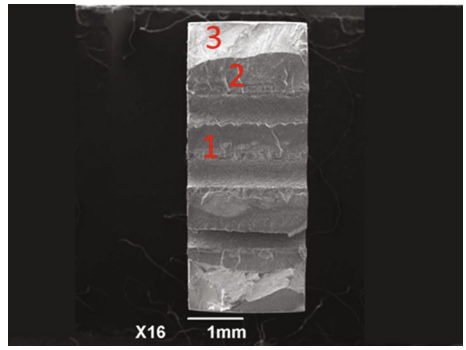

(a) Fracture morphology

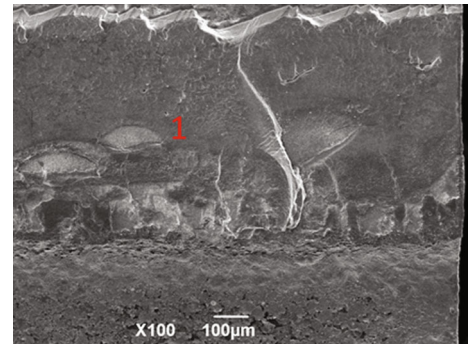

(b) Enlarged morphology of crack initiation region

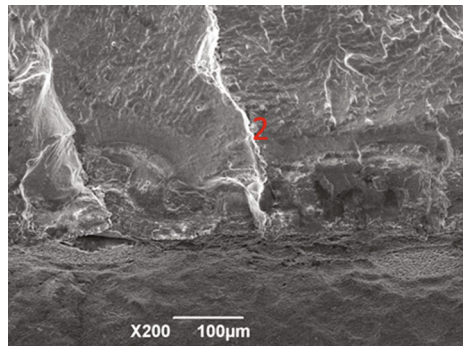

(c) Enlarged morphology of crack propagation region

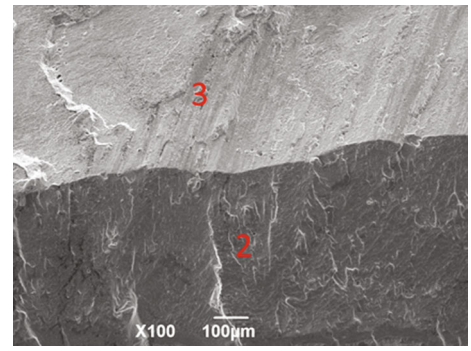

(d) Enlarged morphology of fatigue rupture region

Figure 11: Fracture morphology of multihole specimen.

demonstrate dark gray appearance because of the longer time exposition to oxygen. On the contrary, the final fatigue rupture region is light gray. More importantly, the fracture morphology shows a trapezoid shape, and the hole diameter is not uniform along the thickness direction. Besides, the propagation area of the large hole section is much larger than that of the small hole, indicating that the large hole section propagates earlier than other parts.

A closer inspection on the microscopic appearance of the crack initiation region is depicted in Figure 10(b). The specimen structural integrity is damaged due to the existence of the film cooling holes. Consequently, the crack originated from the defects at the hole edge. Multisource cracks such as 4 and 5 in the figure are generated and propagated until rupture. Meanwhile, the enlarged morphology of the propagation region indicates that the cracks propagate in the normal direction to the tensile stress. Also, the crack propagation implies a typical river-like feature. Finally, the micromorphology of the final fatigue rupture region is presented in Figure 10(d). This area is rough, and stepped tearing characteristics are observed. The failure analysis of the single-hole specimen uncovers that the failure belongs to typical multisource fatigue rupture.

Similar to the single-hole specimen failure analysis results, the crack initiation region, propagation region, and final rupture region of the multihole specimen are presented in Figure 11(a). However, due to the interference effects of the multiholes, the stress distribution of the specimen is complex than the single-hole specimen. Consequently, there are two propagation regions 1 and 2 found in the morphology. Region 1 represents the crack propagating from the interhole whereas region 2 means the crack propagating from the hole edges. The enlarged morphology of region 1 is depicted in Figure 11(b). The crack originates from the faults of the inter hole area and belongs to multisource crack. On one hand, closer inspection shows that there are many radiated lines in the propagation region. The cracks gradually merged due to the stress and converged to a shell-shaped fracture. The color of this area is dark since it is exposed to the oxygen for long time. On the other hand, the cracks propagate along the dangerous path and incorporate the cracks initiating from the hole edge, as shown in Figure 11(c). The sharp drop in the cross-section area of the specimen results in the significant decrease in stress, and the hole around region 2 appears to be ruptured. As a result, the river-like and stepped tearing characteristics are observed. Finally, as shown in Figure 11(d), the fatigue rupture region 3 is in light gray color, indicating that oxidation effect did not occur. Moreover, the coupling effects of oxidation and fatigue stress make the recast layer falling off and becoming rough. It is especially the case in the middle hole of the specimen. The rupture of the multihole specimen is also multisource fatigue rupture.

Table 4: Parameters of the Basquin equation.

Specimen style	σ_f'	b
Single hole, 900°C	1134	-0.052
Single hole, 980°C	1544	-0.076
Single hole, 1050°C	2523	-0.128
Multihole, 980°C	964	-0.060

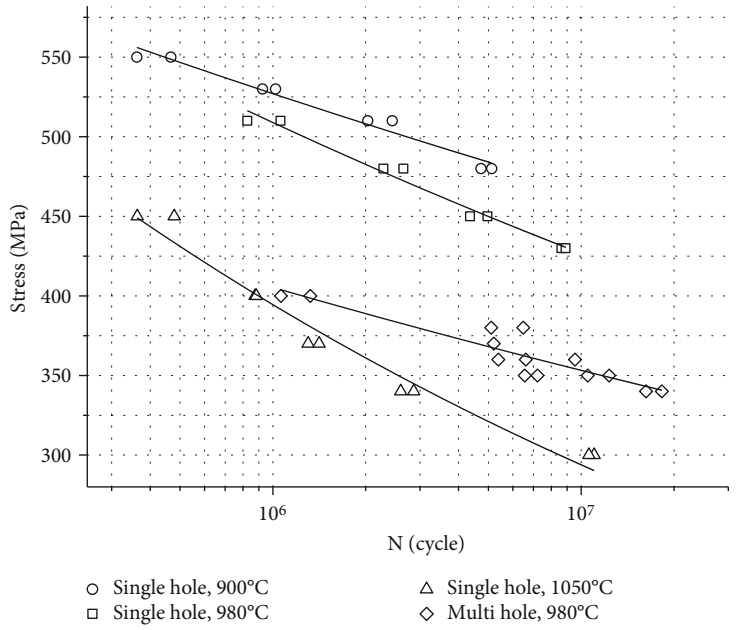

Figure 12: Fitted S-N curve.

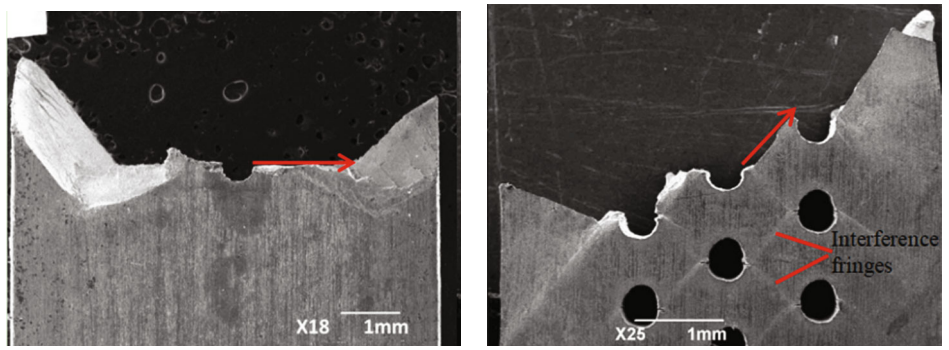

(a) Single-hole results (b) Multihole results

Figure 13: Tested dangerous path demonstration.

4.2. Test Result Analysis. The test results of the single-hole and multihole specimens are fitted using the Basquin equation, as listed in

$$\sigma_a = \sigma_f' \left(2N_f\right)^b. \tag{29}$$

In the above equation, σ_a is the stress amplitude, σ_f' is the fatigue strength coefficient of the material, and b is the Basquin coefficient. The parameters of the Basquin equation are shown in Table 4.

The fitted Basquin equations are demonstrated in the following equations:

$$\begin{aligned} \sigma_{a(900)} &= 1134\left(2N_f\right)^{-0.052}, \\ \sigma_{a(980)} &= 1544\left(2N_f\right)^{-0.076}, \\ \sigma_{a(1050)} &= 2523\left(2N_f\right)^{-0.128}, \\ \sigma_{a-mh} &= 964\left(2N_f\right)^{-0.060}. \end{aligned} \tag{30}$$

The fitted S-N curve implementing the tested data is shown in Figure 12. As expected, the cycle life of the specimen decreases with the increase in rupture stress. For the single-hole specimen, the rupture stress significantly dropped for the higher temperature case. For example, the rupture stress of 10^6 cycles would go down from 525 MPa to 390 MPa when temperature increases from 900°C to 1080°C. Another observation is that the cycle life of the multihole specimen is much lower than that of single-hole specimen under the same temperature.

4.3. Result Comparisons. Figure 13 shows the fracture specimen fracture morphology after HCF experiment under the condition of 980°C/400 MPa. The fracture surface of the specimen shows that for the single-hole specimen, the crack first occurs at the hole edge and then propagates along the [001] plane. The crack front is normal to the tensile axis and then ruptured instantly under tensile stress, as shown in Figure 13(a). For the multihole specimen, the crack propagates gradually along the path between the two holes on the

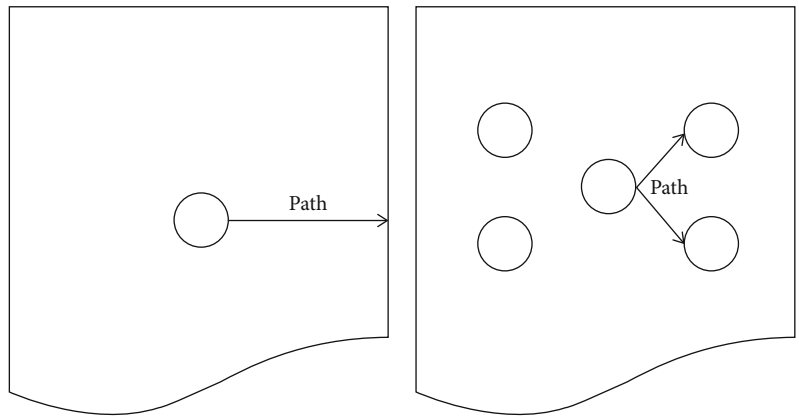

Figure 14: Simplified dangerous paths.

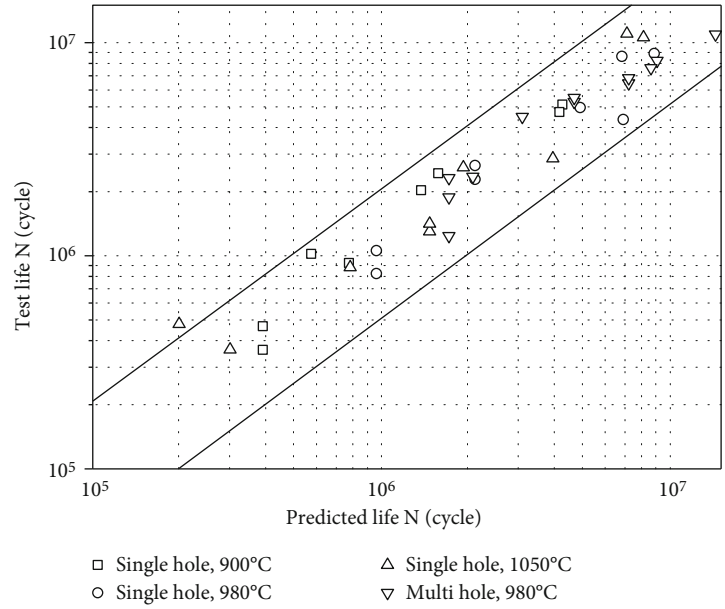

Figure 15: Cycle life comparison between prediction and test.

[101] and [-101] surface and finally ruptures with another hole due to the interhole interference. In the unbroken area, the existence of interference fringes can be observed, which also proves that the crack propagated along the path between holes.

The dangerous paths of the two types of specimens are depicted in Figure 14. It is achieved by the test results. Obviously, the dangerous path of the single-hole specimen is a straight line normal to the tensile axis along the circumference of the hole. On the contrary, the dangerous path of the multihole specimen was the line between the middle hole and the edge hole. It is generated due to the interference of the inner holes.

The relationship between the predicted HCF life and the experimental HCF life is shown in Figure 15. It can be seen that most of the predicted life results implementing MTCD method locate within the twice error band, indicating that the proposed method is capable of estimating the HCF life of specimens with film cooling holes under high temperature conditions.

5. Conclusion

This paper performs a comprehensive investigation on the fatigue life prediction of the turbine blade with film cooling holes. The MTCD was proposed taking the notch effect into consideration. The main outcomes are as follows:

(1) The MTCD method considers both the notch sensitivity and multiaxial stress effects by introducing two parameters. Then, it is implemented in the specimen fatigue life prediction iterations. Both the life of single-hole specimen and multihole specimen are predicted and verified by the tests. Comparison

results show that most of the calculated fatigue life is within the twice error band of the tested life

(2) Failure analysis shows that both the single-hole specimen and multihole specimen ruptured due to fatigue failure. The stress concentration and multiaxial stress resulting from the film cooling holes are the primary reasons that the cracks originated. The cracks then propagated along the dangerous path and resulted in failure

(3) The dangerous path of the single-hole specimen is quite different from the multihole specimen. The crack first appears at the hole edge and propagates along the [001] plane. The crack front is normal to the tensile axis and then ruptured instantly under tensile stress. However, for the multihole specimen, the crack propagates gradually along the path between the two holes on the [101] and [-101] surface and finally ruptures with another hole due to the interhole interference

Nomenclature

Roman Symbols

D: Deformation rate tensor
D_{LM}: Critical distance of line method
D_{PM}: Critical distance of point method
E: Elastic modulus
F: Total deformation gradient
F^e: Elastic deformation gradient
F^p: Plastic deformation gradient
G: Shear modulus
h_0: Hardening modulus
K_f: Theoretical stress concentration factor
K_{IC}: Plane fracture toughness of the material
K_t: Fatigue strength ratio of smooth to notched specimens
ΔK_{th}: Critical stress intensity gradient
L: Characteristic distance
L_0: Critical distance
L_{Nf}: Critical distance under cyclic loading condition
L_S: Critical distance under static loading condition
m: Strain rate sensitivity
$m^{(\alpha)}$: Lattice vector changes and the slip direction
N_0: Initial stage fatigue life
N_S: Fatigue life of static loading condition
N_f: Fatigue life
$n^{*(\alpha)}$: Normal vector
$P^{(\alpha)}$: Schmidt factor of slip system
q_f: Notch sensitivity coefficient
W: Rotation tensor.

Greek Symbols

β: Correction parameter
σ: Cauchy stress tensor
σ_1: Maximum principal stress
σ_{ref}: Reference equivalent stress
σ_{eff}: Equivalent stress
σ_0: Material fatigue limit
σ_{UTS}: Ultimate stress
σ_y: Yield stress
γ: Cumulative slip strain
$\dot{\gamma}^{(\alpha)}$: Reference shear strain rate
$g^{(\alpha)}$: Reference shear stress
h_β: Hardening rate
$q_{\alpha\beta}$: Hardening coefficient
λ: Multiaxial stress factor
τ: Weighed Cauchy stress tensor
τ_s: Correction stress
μ: Poisson's ratio.

Acronyms

AM: Area method
HCF: High cycle fatigue
HSV: Highly stressed volume
LM: Line method
MSCL: Maximum stress concentration location
MTCD: Modified theory of critical distance
PM: Point method
TCD: Theory of critical distance
TET: Turbine entry temperature
VM: Volume method.

Data Availability

The raw/processed data required to reproduce these findings cannot be shared at this time as the data also forms part of an ongoing study.

Conflicts of Interest

The authors declare that they have no conflicts of interest.

Acknowledgments

The authors would like to thank AECC Shenyang Engine Research Institute for the funding and support.

References

[1] D. Mo, I. Roumeliotis, C. Mourouzidis, S. Kissoon, and Y. Liu, "Assessment of performance boundaries and operability of low specific thrust GUHBPR engines for EIS2025," *Journal of Engineering for Gas Turbine and Power*, vol. 144, no. 7, article 071002, 2022.

[2] C. Bagni, *Formalisation of a Novel Finite Element Design Method Based on the Combined Use of Gradient Elasticity and the Theory of Critical Distance, [Ph.D. Thesis]*, The University of Sheffield, 2017.

[3] Q. Miao, W. Ding, W. Kuang, and C. Yang, "Comparison on grindability and surface integrity in creep feed grinding of GH4169, K403, DZ408 and DD6 nickel-based superalloys," *Journal of Manufacturing Processes*, vol. 49, pp. 175–186, 2020.

[4] X. Li, W. Li, M. I. Lashari et al., "Fatigue failure behavior and strength prediction of nickel-based superalloy for turbine

blade at elevated temperature," *Engineering Failure Analysis*, vol. 136, article 106191, 2022.

[5] M. Hüls, P. V. Scheidt, and J. Wallaschek, "Influence of geometric design parameters onto vibratory response and HCF safety for turbine blades with friction damper," in *Proceedings of the ASME Turbo Expo 2018: Turbomachinery Technical Conference and Exposition. Volume 7C: Structures and Dynamics*, Oslo, Norway, 2018.

[6] S. P. Zhu, P. Yue, Z. Y. Yu, and Q. Wang, "A combined high and low cycle fatigue model for life prediction of turbine blades," *Materials*, vol. 10, no. 7, p. 698, 2017.

[7] W. Maktouf, K. Ammar, B. Naceur, and K. Saï, "Multiaxial high-cycle fatigue criteria and life prediction: application to gas turbine blade," *International Journal of Fatigue*, vol. 92, no. 1, pp. 25–35, 2016.

[8] H. Neuber, *Theory of Notch Stresses: Principles for Exact Calculation of Strength with Reference to Structural Form and Material*, Springer, Berlin, 2nd edition, 1958.

[9] E. Peterson, "Notch sensitivity," in *Metal Fatigue*, G. Sines and J. L. Waisman, Eds., pp. 293–306, McGraw Hill, New York, 1969.

[10] L. Susmel and D. Taylor, "Fatigue design in the presence of stress concentrations," *Journal of Strain Analysis for Engineering Design*, vol. 38, no. 5, pp. 443–452, 2003.

[11] D. Taylor, *The Theory of Critical Distances: A New Perspective in Fracture Mechanics*, Elsevier, Oxford, UK, 2007.

[12] D. Taylor, "The theory of critical distances," *Engineering Fracture Mechanics*, vol. 75, no. 7, pp. 1696–1705, 2008.

[13] D. Taylor and G. Wang, "The validation of some methods of notch fatigue analysis," *Fatigue & Fracture of Engineering Materials & Structures*, vol. 23, no. 5, pp. 387–394, 2000.

[14] L. Susmel, "A unifying approach to estimate the high-cycle fatigue strength of notched components subjected to both uniaxial and multiaxial cyclic loadings," *Fatigue & Fracture of Engineering Materials & Structures*, vol. 27, no. 5, pp. 391–411, 2004.

[15] C. Santus, "Fretting fatigue of aluminum alloy in contact with steel in oil drill pipe connections, modeling to interpret test results," *International Journal of Fatigue*, vol. 30, no. 4, pp. 677–688, 2008.

[16] L. Bertini and C. Santus, "Fretting fatigue tests on shrink-fit specimens and investigations into the strength enhancement induced by deep rolling," *International Journal of Fatigue*, vol. 81, pp. 179–190, 2015.

[17] J. A. Araújo, F. C. Castro, S. Pommier, J. Bellecave, and J. Meriaux, "On the design and test of equivalent configurations for notch and fretting fatigue," *Fatigue & Fracture of Engineering Materials & Structures*, vol. 39, no. 10, pp. 1241–1250, 2016.

[18] J. A. Araújo, L. Susmel, M. S. T. Pires, and F. C. Castro, "A multiaxial stress-based critical distance methodology to estimate fretting fatigue life," *Tribology International*, vol. 108, pp. 2–6, 2017.

[19] J. A. Araújo, G. M. J. Almeida, J. L. A. Ferreira, C. R. M. da Silva, and F. C. Castro, "Early cracking orientation under high stress gradients: the fretting case," *International Journal of Fatigue*, vol. 100, pp. 611–618, 2017.

[20] C. Ronchei, A. Carpinteri, G. Fortese, D. Scorza, and S. Vantadori, "Fretting high-cycle fatigue assessment through a multiaxial critical plane-based criterion in conjunction with the Taylor's point method," *Solid State Phenomena*, vol. 258, pp. 217–220, 2016.

[21] M. Benedetti, V. Fontanari, C. Santus, and M. Bandini, "Notch fatigue behaviour of shot peened high-strength aluminium alloys: experiments and predictions using a critical distance method," *International Journal of Fatigue*, vol. 32, no. 10, pp. 1600–1611, 2010.

[22] M. Benedetti, V. Fontanari, M. Allahkarami, J. C. Hanan, and M. Bandini, "On the combination of the critical distance theory with a multiaxial fatigue criterion for predicting the fatigue strength of notched and plain shot-peened parts," *International Journal of Fatigue*, vol. 93, pp. 133–147, 2016.

[23] L. Susmel, "The theory of critical distances: a review of its applications in fatigue," *Engineering Fracture Mechanics*, vol. 75, no. 7, pp. 1706–1724, 2008.

[24] L. Susmel and D. Taylor, "A simplified approach to apply the theory of critical distances to notched components under torsional fatigue loading," *International Journal of Fatigue*, vol. 28, no. 4, pp. 417–430, 2006.

[25] L. Susmel, "High-cycle fatigue of notched plain concrete," *Procedia Structural Integrity*, vol. 1, pp. 2–9, 2016.

[26] D. Liao, S. P. Zhu, and G. Qian, "Multiaxial fatigue analysis of notched components using combined critical plane and critical distance approach," *International Journal of Mechanical Science*, vol. 160, pp. 38–50, 2019.

[27] S. P. Zhu, W. L. Ye, J. A. F. O. Correia, A. M. P. Jesus, and Q. Wang, "Stress gradient effect in metal fatigue: review and solutions," *Theoretical and Applied Fracture Mechanics*, vol. 121, article 103513, 2022.

[28] J. C. He, S. P. Zhu, A. T. Taddesse, and X. Niu, "Evaluation of critical distance, highly stressed volume, and weakest-link methods in notch fatigue analysis," *International Journal of Fatigue*, vol. 162, article 106950, 2022.

[29] O. Jadallah, C. Bagni, H. Askes, and L. Susmel, "Microstructural length scale parameters to model the high-cycle fatigue behaviour of notched plain concrete," *International Journal of Fatigue*, vol. 82, pp. 708–720, 2016.

[30] D. H. Chen, "Consideration to the mean stress based line method for estimating the notch fatigue limit," *Theoretical and Applied Fracture Mechanics*, vol. 112, article 102921, 2021.

[31] S. M. J. Razavi, H. Askes, F. Berto, and L. Susmel, "Length scale parameters to estimate fatigue lifetime of 3D-printed titanium alloy Ti6Al4V containing notches in the as-manufactured condition," *International Journal of Fatigue*, vol. 167, article 107348, 2023.

[32] D. Shi, C. Dong, and X. Yang, "Constitutive modeling and failure mechanisms of anisotropic tensile and creep behaviors of nickel-base directionally solidified superalloy," *Materials & Design*, vol. 45, pp. 663–673, 2013.

[33] G. Han, J. Yu, X. Sun, and Z. Hu, "Effect of threshold stress on anisotropic creep properties of single crystal nickel-base superalloy SRR99," *Journal of Materials Science & Technology*, vol. 28, no. 5, pp. 439–445, 2012.

[34] R. Hill, "Generalized constitutive relations for incremental deformation of metal crystals by multislip," *Journal of the Mechanics and Physics of Solids*, vol. 14, no. 2, pp. 95–102, 1966.

[35] R. Hill and J. R. Rice, "Constitutive analysis of elastic-plastic crystals at arbitrary strain," *Journal of the Mechanics and Physics of Solids*, vol. 20, no. 6, pp. 401–413, 1972.

[36] G. I. Taylor, "The mechanism of plastic deformation of crystals. Part I.—Theoretical," *Proceedings of the Royal Society of*

London. Series A, Containing Papers of a Mathematical and Physical Character, vol. 145, no. 855, pp. 362–387, 1934.

[37] G. I. Taylor, "The mechanism of plastic deformation of crystals. Part II.—Comparison with observations," *Proceedings of the Royal Society of London. Series A, Containing Papers of a Mathematical and Physical Character*, vol. 145, no. 855, pp. 388–404, 1934.

[38] L. Susmel and D. Taylor, "The theory of critical distances to estimate finite lifetime of notched components subjected to constant and variable amplitude torsional loading," *Engineering Fracture Mechanics*, vol. 98, pp. 64–79, 2013.

[39] B. Z. Wang, D. S. Liu, Z. X. Wen, and Z. F. Yue, "Tension/compression asymmetry of [001] single-crystal nickel-based superalloy DD6 during low cycle fatigue," *Materials Science and Engineering: A*, vol. 593, pp. 31–37, 2014.

[40] Z. Wen, H. Pei, C. Zhang, and B. Wang, "Analysis of surface quality of multi-film cooling holes in nickel-based single crystal superalloy," *Materials Science and Technology*, vol. 32, no. 18, pp. 1845–1854, 2016.